Wicking Study of Nanostructured Titania Surfaces for Flat Heat Pipes

C. Ding , G. Soni, P. Bogorzi, C. Meinhart and N.C. MacDonald

Room 2229, ESB, University of California
Santa Barbara, CA, USA, ding@engr.ucsb.edu

ABSTRACT

We report a wicking material based on nanostructured TiO_2 (NST) for the application of flat heat pipes. Heat pipes adopt wicking materials to achieve some unique functions that thermal siphons could not achieve[1], and they have found their applications as cooling systems in a wide variety of areas such as spacecraft and electronics. Different kinds of materials such as carbon nanotubes[2], nanowires[3], sintered copper[4], and micromachined channels[5, 6] have been investigated for micro heat pipes for their wicking functions. Based on titanium micromachining and surface modification techniques, we fabricated an array of pillars which carry nano/micro textured surface Our study shows that water can completely wet this nano/micro textured surface, and it's wetting behavior on this surface follows the famous Washburn equation.

Keywords: titanium, nanostructure, wetting, wick, heat pipe

1 WETTING PHYSICS

Vapor, liquid and solid are common material phases that we see in our life, and it's very common that these three phases stay together either statically or dynamically. For whatever shape or volume the materials take, their sizes are limited so that they have surfaces or interface(s) between each other. These surfaces or interfaces carry unsatisfied bonds forming surface energy or interface energy[7], and their relative values, together with the surface roughness/microstructures determine the contact behavior of a droplet on a solid surface[8]. Wetting and hydrophobicity on solid surfaces are important phenomena to study for applications such as heat pipe[1, 4], self-cleaning glasses, inkjet printing, DNA chips[9], etc..

1.1 Wetting with roughness

For a droplet sitting on a smooth and flat surface (Fig1a), hydrophobicity or wetting is governed by the relative reaction of the forces at the triple line arising from the three interfacial tensions (or call surface energy), γ_{SV}, γ_{SL}, and γ, taking place at the solid-vapor, solid-liquid, and liquid-vapor interfaces, respectively. Projecting these three surface tensions acting on a specific contact line gives the Young's equation:

$$\cos\theta_e = \frac{\gamma_{SV} - \gamma_{SL}}{\gamma} \quad (1)$$

where θ_e is the equilibrium contact angle. Different regimes can be obtained, together with the asymmetry between the hydrophilic side ($\theta_e < \pi/2$), and hydrophobic side ($\theta_e > \pi/2$). In the hydrophobic regime, θ_e is larger than $\pi/2$. With this condition, the drop sits on the top of the rough or textured surface, and air is trapped under the drop.

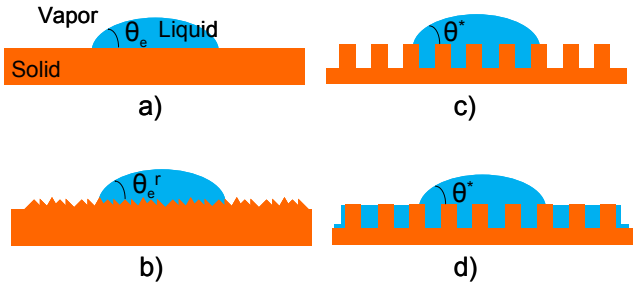

Fig. 1: a) Droplet on a smooth and flat surface; b) droplet on a practical rough surface; c) the triple line is pinned on islands; d) corresponding to film regime in which the micro/nano structures outside the drop is filled with a liquid.

However, solid surfaces are usually rough or carry undulations, pores, surface defects. Denoting by r the roughness of the solid surface (the ratio of the total surface area over the projected one), a displacement dx of the contact line implies a change in the total surface energy per unit length:

$$dE = r(\gamma_{SL} - \gamma_{SV})dx + \gamma dx\cos\theta_e^r \quad (2)$$

where E is minimal at the equilibrium, then we have:

$$\gamma\cos\theta_e^r = r(\gamma_{SL} - \gamma_{SV}) \quad (3)$$

Together with Young's equation, above equation leads to Wenzel's relation[10]:

$$\cos\theta_e^r = r\cos\theta_e \quad (4)$$

where θ_e^r is the apparent contact angle. For flat surface, $r=1$, and above equation stay valid. For rough surfaces, $r>1$. Analytically, this relation is limited to the case $-1 \le r\cos\theta_e \le 1$ implying that once r is too large this relation does not apply for the reason of $-1 \le \cos\theta_e^r \le 1$. However, it does tell us that the surface roughness can enhance both the nonwetting (hydrophobic) and wetting (hydrophilic) ability of liquid on solid surfaces[11-13]. When the Young's contact angle on flat/smooth surface is less than 90°, roughness will reduce the apparent contact angle leading to superhydrophilic/superwetting case[3, 14, 15]. If the Young's contact angle is larger than 90°, the roughness will increase the apparent contact angle, leading to superhydrophic/super-Antiwetting case [14]. The Wenzel's equation also predicts that complete wetting can be achieved for all partial wetting liquids satisfying $\cos\theta_e > 1/r$ [12], corresponding to $dE<0$.

1.2 Micro-textured surface effect on wetting

The topography enhancement for both wetting and nonwetting has been studied extensively. We showed in the previous subsection that the roughness modifies the value of apparent contact angle, and superwetting can possibly be achieved by tuning the roughness. We use micromachined pillars (Fig. 1c, Fig. 1d) to modify the surface roughness, which can be tuned to optimize the wetting by adjusting the pillar dimensions. We denote the surface by its pillar density ϕ_s and roughness r. Provided that the case of wetting as in Fig. 2, the pillars guide the liquid within the pillar arrays and form in a manner similar to wicking but more accurately hemiwicking which is intermediate between spreading and imbibition [8]. For the liquid front boundary progressing by a distance *dx*, the variation of the surface energy per unit length vertical to the figure is:

$$dE = (\gamma_{SL} - \gamma_{SA})(r - \phi_s)dx - \gamma(1-\phi_s)dx \tag{5}$$

For the progression to be favorable (*dE*<0), together wtih Young's equation, we have

$$\cos\theta > \frac{1-\phi_s}{r-\phi_s} = \cos\theta_c \tag{6}$$

where θ_c is defined as the critical angle and:

$$r = 1 + \frac{2\pi bh}{p^2} \tag{7}$$

Provided that $\theta < \theta_c$, the hemiwicking will take place. When $r >> \phi_s$, we obtain $\cos\theta_c \approx 1/r$, which means the rough surface is preferred for hemiwicking of wetting liquids. The propagation of the wetting liquids is made possible via the menisci that form around each pillar, allowing the liquid to reach their neighbor ones. The equilibrium contact angle can be derived by considering a virtual displacement *dx* of the contact line leading to the fraction of the surface (top surface) ϕ_s, elimination on the liquid-vapor interface of a fraction $1-\phi_s$, and an increase of the liquid-vapor interface of the drop. The total surface energy change finally can be express as:

$$dE = \phi_s(\gamma_{SL} - \gamma_{SA})dx - (1-\phi_s)\gamma dx + \gamma\cos\theta^* dx \tag{8}$$

The equilibrium stays at *dE*=0, together with Young's relation, leading to the Cassie equation[16]:

$$\cos\theta^* = 1 - (1-\phi_s)\cos\theta_e \tag{9}$$

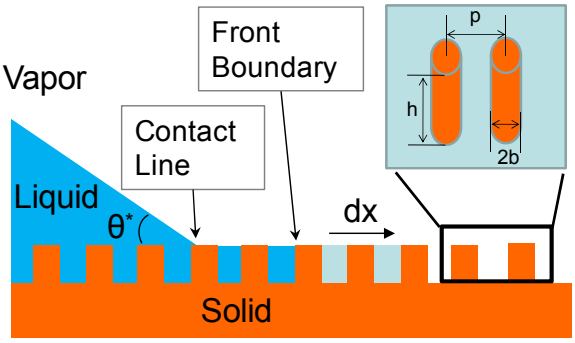

Fig. 2: Flow of the impregnating film at the front boundary. The precursor film was formed by a molecular liquid layer. As it progresses by *dx* and coat the nano/micro structured surfaces, it replaced the solid-air surface energy by with the solid liquid energy. A negative energy change takes place, and complete wetting is formed with this progression.

1.3 Dynamics of wetting

The driving force for hemiwicking is given by

$$F = -dE/dx = \gamma(r-\phi_s)(\cos\theta_e - \cos\theta_c) \tag{10}$$

which is derived from equation (5) in which case the top surfaces of the pillars are dry when the liquid film propagates. Due to the precursor film, the top surface areas can also wet during the progression of the liquid film. Then the surface energy change is only due to the suppression of the liquid-vapor interfaces. In this case the force shall be given by:

$$F = \gamma(r-1) = \frac{2\pi\gamma bh}{p^2} \tag{11}$$

The driving force is then constant and it depends only on the surface roughness. Resistance to flow results from viscous losses that occur due to no-slip on the lower

NSTI-Nanotech 2009, www.nsti.org, ISBN 978-1-4398-1784-1 Vol. 3, 2009

surfaces and the pillars. Because of the geometrical complexity, no simple analytical expression for viscous losses exists to our knowledge. Washburn [17] analyzed a simple tube-shaped geometry. By balancing the capillary driving force with the viscous resistance, he was able to deduce the Washburn relation for interface velocity,

$$\frac{dx}{dt} = \frac{w\gamma \cos\theta}{4\eta} \frac{1}{x}, \qquad (12)$$

where w is the characteristic length of the system. Washburn relation [17] which stipulates that the travel path of the flow increases as the square root of time: $x = (Dt)^{1/2}$, where D is defined as the dynamic coefficient of the flow. A high dynamical coefficient is preferred for the wicking material (pillar arrays) used in the proposed heat pipe (Fig. 3) for carrying high heat capacity.

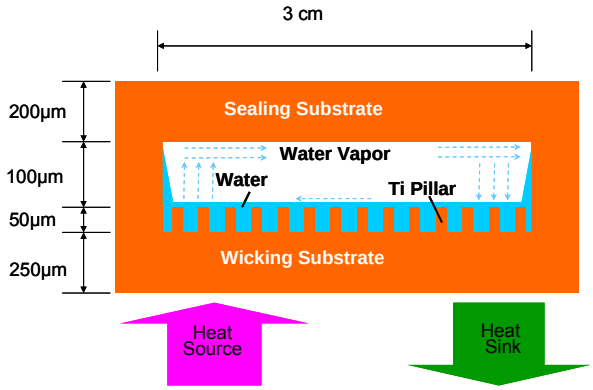

Fig. 3: Schematic of the Ti-based heat pipe. The overall device is less than 1 mm thick. The micro pillar arrays are super hydrophilic and form the wicking material.

2 FABRICATION OF PILLAR ARRAYS

The fabrication process for making Ti pillars (Fig. 4) begins with the SiO_2-masked deep etching of a 300 µm thick Ti substrate using Inductively Coupled Plasma (ICP) etch in an Ar/Cl_2 ambience. The SiO_2 layer is approximately 3 µm thick. After deep etching is complete, the sample is oxidized in a 30% solution of hydrogen peroxide at 83 ^{0}C to obtain the Nano-structured Titania (NST) hair at the pillar surfaces and the bottom floor surface (Fig. 5). The NST surfaces shows nano-scale walls (30~50nm thick) and pores (150~200nm in diameter). The NST structures are self assembled on high-aspect-ratio Ti pillar arrays when oxidized in H_2O_2 solution.

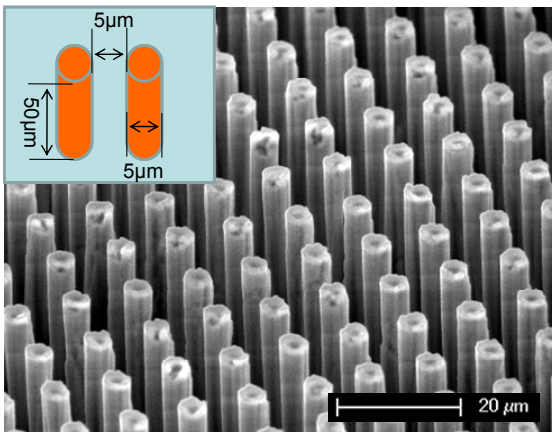

Fig. 4: SEM photograph of the high aspect ratio bulk Ti pillar arrays. The height of the pillars is about 50µm.

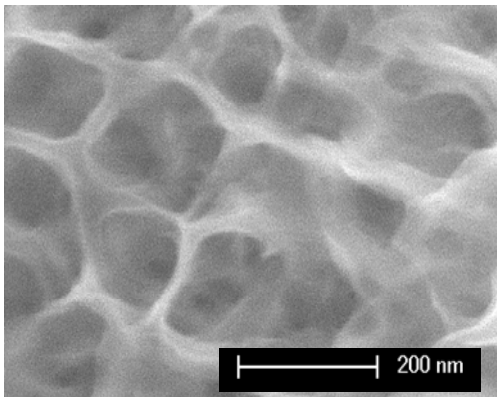

Fig. 5: SEM photograph of the nanostructured titania (NST) on the high aspect ratio bulk Ti pillars. Such nanosturctured surfaces covers all the pillar surfaces and the bottom floor surface.

3 EXPERIMENT

We used DI water as a working fluid for the wicking test. The experiment was done by bringing our samples into contact with a drop of water (~14µL), and the flow is recorded with a camera. The positions of the front boundary were extracted by decomposing the video into 15 frames/second. Figure 6 shows the propagation of the front boundary at different snap shots. The drop size shrinks along the progression of the liquid film. Travel distance measurements count in the shrinkage of the drop.

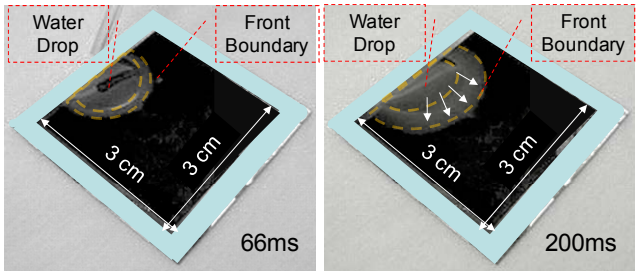

Fig. 6: Hemiwicking material was tested by placing a drop of water (14 µL) at one edge of the wicking substrate. The inside half circle shows the drop forms a reservoir for the hemiwicking flow, and the outside half circle shows the front boundary of the liquid film. The drop completely wetted the nano/micro structured surface at the end, and the contact angle goes to zero.

4 ANALYSIS AND DISCUSSION

A curve of the form $x^2 = Dt$ is fitted to the collected distance-vs-time data shown in Fig. 7. The experimental data generate a dynamic coefficient $D = 1.1\times10^{-4}$ m^2s^{-1}. In other words, $x = 10.5\times10^{-3}t^{1/2}$.

By differentiating the above equation we get the spreading speed:

$$\frac{dx}{dt} = \frac{5.5125\times10^{-5}}{x} \qquad (13)$$

This equation shows that the spreading velocity of the flow is proportional to the inverse of the traveling distance. The verifies that the water flow on this nanostructured titania surface follows the Washburn rule. Note that the water travels 10mm within less than 1 second in the nanostructured titania pillar arrays.

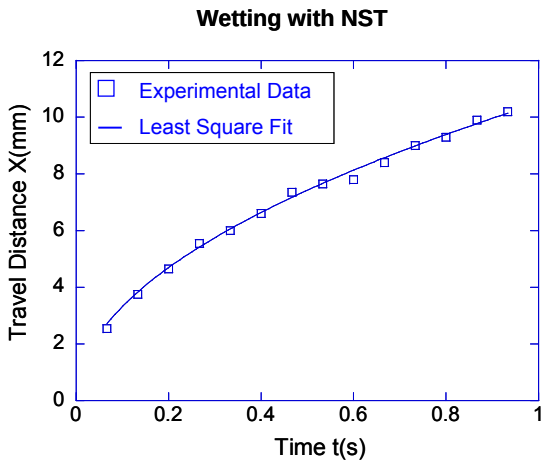

Fig. 7: This plot shows the capillary flow front boundary path as a function of time. Water was used as a working fluid. As shown the front boundary travels ~10mm within 1 second.

5 CONCLUSION

A high-performance wick was created by etching micro pillars in titanium and by growing hair-like Nano-Structured Titania (NST) on the pillar surface. A very high hemiwicking flow velocity of ~10 mm/s was obtained over a ~10 mm length using water as wetting fluid on nano/micro textured surfaces. Complete wetting of water on the pillar arrays was observed on a 3cmX3cm square sample. Washburn's theory of capillary flow was used to analyze the experimental results. It was found that the experimental data agrees well with the Washburn relation. By optimizing the geometry of the wicking structure, one can significantly improve the performance of the wick design.

This work is supported by the Microsystems Technology Office at the Defense Advanced Research Projects Agency. A portion of this work was done in the UCSB nanofabrication facility, part of the NSF funded NNIN network.

REFERENCE

[1] Dunn, P.D. and D.A. Reay, *Heat pipe.* Physics in Technology, 1973. **4**(3): p. 187-201.

[2] Vadakkan, U., et al. *A Novel Carbon Nano Tube based Wick Structure for Heat Pipes/Vapor Chambers*. in *SEMI-THERM 2007. Twenty Third Annual IEEE*. 2007.

[3] Yuan, J., et al., *Superwetting nanowire membranes for selective absorption.* Nature Nanotechnology, 2008. **3**(6): p. 332.

[4] Mariana, L., et al. *Metallic Porous Parts for Electronics Devices Cooling*. in *Electronics Systemintegration Technology Conference, 2006. 1st*. 2006.

[5] Joo, Y., K. Dieu, and C.J. Kim, *Fabrication of Monolithic Microchannels for IC Chip Cooling.* An Investigation of Micro Structures, Sensors, Actuators, Machines and Systems, 1995: p. 362-7.

[6] Linan, J., et al., *Closed-loop electroosmotic microchannel cooling system for VLSI circuits Closed-loop electroosmotic microchannel cooling system for VLSI circuits.* Part A: Packaging Technologies, IEEE Transactions on], 2002. **25**(3): p. 347-355.

[7] Israelachvili, J.N., *Intermolecular and surface forces*. 1992, Academic Press London.

[8] QuÃ©rÃ©, D., *Wetting and Roughness.* Annual Review of Materials Research, 2008. **38**(1): p. 71-99.

[9] Blanchard, A.P., R.J. Kaiser, and L.E. Hood, *High-density oligonucleotide arrays.* Biosensors and Bioelectronics, 1996. **11**(6-7): p. 687-690.

[10] Wenzel, R.N., *RESISTANCE OF SOLID SURFACES TO WETTING BY WATER.* Industrial & Engineering Chemistry, 1936. **28**(8): p. 988-994.

[11] Bico, J., U. Thiele, and D. Quéré, *Wetting of textured surfaces.* Colloids and Surfaces A: Physicochemical and Engineering Aspects, 2002. **206**(1-3): p. 41-46.

[12] McHale, G., et al., *Topography Driven Spreading.* Physical Review Letters, 2004. **93**(3): p. 036102.

[13] Bico, J., C. Tordeux, and D. Quere, *Rough wetting.* Europhysics Letters, 2001. **55**(2): p. 214-220.

[14] Feng, X. and L. Jiang, *Design and creation of superwetting/antiwetting surfaces.* Adv. Mater, 2006. **18**: p. 3063-78.

[15] Extrand, C., et al., *Superwetting of Structured Surfaces.* Langmuir, 2007. **23**(17): p. 8882-8890.

[16] Cassie, A. and S. Baxter, *Wettability of porous surfaces.* Transactions of the Faraday Society, 1944. **40**: p. 546-551.

[17] Washburn, E.W., *The Dynamics of Capillary Flow.* Physical Review, 1921. **17**(3): p. 273.